

Origin and evolution of ore fluids in the late Mesozoic Naozhi epithermal Au–Cu deposit, Yanbian area, Northeast China: evidence from fluid inclusion and isotopic geochemistry

A-Lei Gu¹ · Lan-jing Men² · Jing-Gui Sun¹ · Keisuke Nagao³ · Ling-An Bai^{1,4} · Long-pei Cui^{1,2,3} · Peng Chai¹ · Yan-jun Chen¹ · Jun-quan Zhu¹

Received: 15 March 2015 / Accepted: 10 September 2015 / Published online: 22 February 2016
© Saudi Society for Geosciences 2015

Abstract The Naozhi Au–Cu deposit is located on the continental margin of Northeast China, forming part of the West Pacific porphyry–epithermal gold–copper metallogenic belt. In this paper, we systematically analyzed the compositions, homogenization temperatures, and salinity of fluid inclusions as well as their noble gas isotopic and Pb isotopic compositions from the deposit. These new data show that (1) five types of fluid inclusions were identified as pure gas inclusions (V-type), pure liquid inclusions (L-type), gas–liquid two-phase inclusions (W-type, as the main fluid inclusions (FIs)), CO₂-bearing inclusions (C-type), and daughter-mineral-bearing polyphase inclusions (S-type); (2) W-type FIs in quartz crystals of early, main, and late stage are homogenized at temperatures of 324.7–406.7, 230–338.8, and 154.6–308 °C, with salinities of 2.40–7.01 wt% NaCl_{eq}, 1.73–9.47 wt% NaCl_{eq}, and 6.29 wt% NaCl_{eq}, respectively. S-type FIs in quartz crystals of early stage are homogenized at temperatures of 328.6–400 °C, with salinities of 39.96–46.00 wt% NaCl_{eq}; (3) Raman analysis results reveal that the vapor compositions of early ore-forming fluids consisted of CO₂

and H₂O, with H₂O gradually increasing and CO₂ being absent at the late mineralization stage; (4) fluid inclusions in pyrite and chalcopyrite have ³He/⁴He ratios of 0.03–0.104 Ra, ²⁰Ne/²²Ne ratios of 9.817–9.960, and ⁴⁰Ar/³⁶Ar ratios of 324–349. These results indicate that the percentage of radiogenic ⁴⁰Ar* in fluid inclusions varies from 8.8 to 15.5 %, containing 84.5–91.2 % atmospheric ⁴⁰Ar; (5) the ²⁰⁶Pb/²⁰⁴Pb, ²⁰⁷Pb/²⁰⁴Pb, and ²⁰⁶Pb/²⁰⁴Pb ratios of sulfides are 18.1822–18.3979, 15.5215–15.5998, and 38.1313–38.3786, respectively. These data combined with stable isotope data and the chronology of diagenesis and metallogenesis enable us to suppose that the ore-forming fluids originated from the melting of the lower crust, caused by the subduction of an oceanic slab, whereas the mineralized fluids were exsolved from the late crystallization stage and subsequently contaminated by crustal materials/fluids during ascent, including meteoric water, and the mineral precipitation occurred at a shallow crustal level.

Keywords Fluid inclusions · Noble gas isotopes · Pb isotopes · Origin and evolution of ore fluids · Naozhi · Epithermal Au–Cu deposit · Yanbian

✉ Lan-jing Men
54361959@qq.com

✉ Jing-Gui Sun
sunjinggui@jlu.edu.cn

¹ College of Earth Sciences, Jilin University, 2199 Jianshe Street, Changchun 130061, China

² Changchun Institute of Technology, Changchun, China

³ Laboratory for Earthquake Chemistry, Graduate School of Science, The University of Tokyo, Tokyo 7-3-1, Japan

⁴ Guangxi Scientific Experiment Center of Mining, Metallurgy and Environment, Guilin University of Technology, Guilin 541004, China

Introduction

Epithermal Cu–Ag deposits are an important part of the epithermal–porphyry copper–gold mineralization systems. These epithermal deposits commonly occur at shallower crustal levels than porphyry type deposits, and Au–Ag mineralization and wall rock alteration take place by distinctively chemically different hydrothermal fluids (Hedenquist and Lowenstern 1994; Cooke and Simmons 2000; Mao et al. 2003; Groves and Bierlein 2007; Sillitoe 2008). Since the 1970s, a number of world class super large-scale epithermal gold (copper) deposits have been discovered in the Circum

Pacific, Mediterranean–Himalaya orogen, and the Mongolia–Okhotsk Belt (Jiang et al. 2004).

Yanbian area is located near the continental margin of Northeast China, containing porphyry deposit (Nongping) or porphyry-like deposit (Xiaoxinancha), epithermal low-sulfidation Au deposits (e.g., Ciweigou, Wufeng, and Wuxingshan), and epithermal medium-sulfidation Cu–Au deposits (e.g., Naozhi and Fuyan) (Fig. 1b). These discoveries indicate the high potential of the area to host epithermal gold–copper deposits (Bing et al. 1995; Meng et al. 2001; Han et al. 2013).

The Naozhi Au–Cu deposit, which belongs to the Yanbian ore district, is located in southern Baicaogou town, Yanbian autonomous prefecture, Jilin Province. Since the discovery of Naozhi during the 1970s, scientists have conducted geological, geochemical, and mineralization investigations of the ore deposit. Few systematic fluid inclusion studies have been performed, although various conflicting hypotheses have been advanced to explain its formation, including a volcanic–subvolcanic hydrothermal origin (Li and Yang 1991) a transition type between epithermal and porphyry (Bing et al. 1995) a medium-temperature magmatic hydrothermal origin (Su et al. 2003; Yang et al. 2010) a low-sulfidation epithermal gold origin (Lin 2013; Wu 2013) and a high-sulfidation epithermal gold deposit (Zhao 2007; Wan 2013). In this contribution, on the basis of previous studies, we present a detailed study of the fluid inclusions hosted in quartz at different ore-forming stages, as well as the noble gas isotopic and Pb isotopic compositions in ore minerals from the deposit, for the purpose of tracing possible fluid sources and mineralization processes of the ore-forming fluids.

Geological background and description of the mineral deposit

Geological background

The location of the Naozhi Cu–Au deposit is shown in Fig. 1. Tectonically, it is situated at the eastern end of the Central Asia Orogenic Belt (CAOB) (Tianshan–Mongolia–Hingan), adjacent to the Jiamusi Massif in the north, the North China Plate in the south, and the Khanka Massif in the northeast (Fig. 1a). This region has undergone a number of significant geological events such as the evolution of the ancient Asian Ocean, the Xing’an–Mongolian orogen, Mesozoic subduction of the paleo-Pacific plate, and Cenozoic supercrustal faulting (Peng and Zhao 2001). The exposed strata in the area comprise Paleozoic epimetamorphic rocks, Mesozoic volcano–sedimentary rocks, and Cenozoic volcanic rocks (Meng et al. 2001; Jin 2003). Four stages of intrusive rocks have been identified in the Yanbian area: Middle–Late Permian gabbro and diorite, Late Permian–Early Jurassic granodiorite and monzogranite,

Middle–Late Jurassic granite, and Early Cretaceous granitoid complex (Meng et al. 2001; Zhang 2002; Sun et al. 2008a, b). Regional structures include Paleozoic E–W-trending ductile deformation zones and Mesozoic or younger faults that trend NNE–SSW, N–S, and NNW–SSE (Fig. 1b).

Ore deposit geology

The Naozhi Cu–Au deposit is an important member of the eastern Yanbian district. The deposit is located in a NW–SE secondary fault system (Fig. 2a). The deposit is hosted by Lower Jurassic granodiorite, biotite monzonitic granite, and quartz diorite and is overlain by Lower Cretaceous volcanic rocks and subvolcanic intrusions (Zhang 2002; Zhang et al. 2004; Han et al. 2013). Geochronology data for the host rocks and alteration minerals show that the monzonitic granite in the mining area is Early Jurassic in age (Zhang 2002; Han et al. 2013) the main vein rocks associated with the ore body are diorite–porphyry of 130–123.3 Ma in age (Han et al. 2013; Lin 2013) and the Jingouling group formed at 123–115 Ma (Jin 2003). Han et al. (2013) obtained a $^{40}\text{Ar}/^{39}\text{Ar}$ plateau age of 128.6 ± 1.4 Ma from secondary sericite, and Meng et al. (2001) obtained a $^{40}\text{Ar}/^{39}\text{Ar}$ isochron age of 123.6 ± 2.5 Ma from quartz-hosted fluid inclusions. The above studies indicate that the Naozhi Au–Cu deposit is related to intermediate–basic magmatism and to subvolcanic, shallow magmatism of the Jingouling stage (Early Cretaceous).

The Naozhi ore body consists of ten subparallel bands of gold-bearing polymetallic sulfide–quartz veins with associated alteration haloes, of which the no. 1, 9, 10, and 20 veins are the largest. The ore body is 350–1,020 m long, 0.4–12.3 m wide, and >450 m deep. The ore bodies display parallel along their length and depth (Fig. 2c). The gold grade of these ore bodies reaches 74.5 g/t. Pyrite and chalcopyrite are the dominant ore minerals, together with sphalerite, galena, tetrahedrite, chalcocite, magnetite, and natural gold, electrum, and petzite (Fig. 3). Texturally, the ores show euhedral–subhedral texture and dissolution metasomatism residual texture, as well as banded, brecciated, massive, vein-like, and veinlet-disseminated structures. Wall rock alteration can be divided into three zones on the basis of alteration type and intensity. The inner zone is pervasive marked by K-feldspathization, sericitization, silicification, carbonatization, and pyritization, and it is a gold-bearing high-grade alteration zone; an intermediate quartz–sericite–pyrite (QSP) zone showing outwards a chlorite enrichment and subsequent quartz, sericite and pyrite impoverishment; and an outer chloritized (propylitic) (Fig. 2b).

Based on ore textures, crosscutting relationships, and mineral assemblages, the hydrothermal mineralization process can be divided into four stages (Fig. 4): (1) The K-feldspar–quartz stage commonly shows various degrees of replacement by pyrite–sericite–quartz veins (Fig. 3b). Minerals in these veins include quartz, K-feldspar, albite, pyrite, sericite with minor

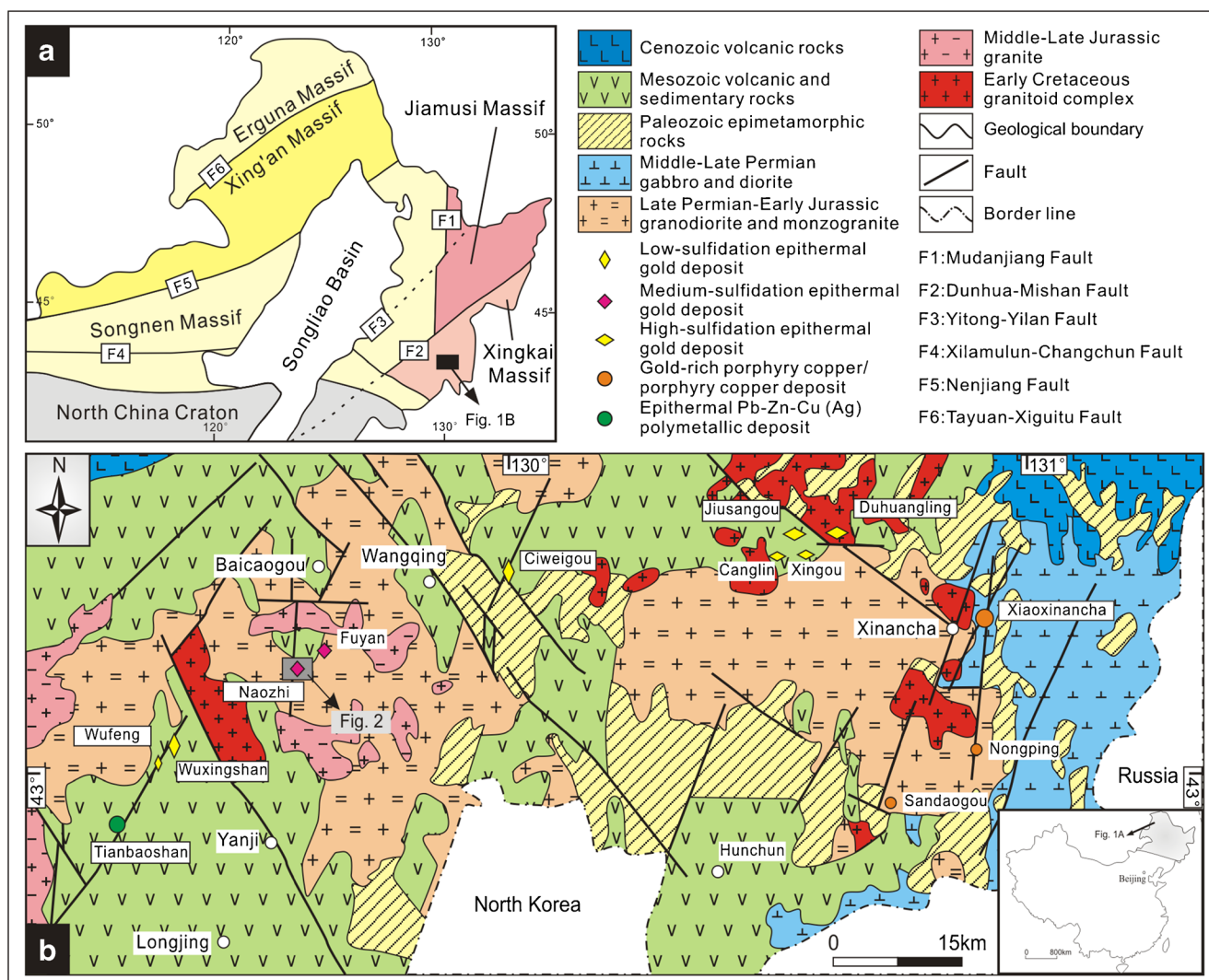


Fig. 1 a Geotectonic divisions in Northeast China (after Wu et al. 2011). b Geological map of the Yanbian area showing the locations of gold or copper deposits (modified from Meng et al. 2001; Chai et al. 2015)

chlorite, and residual magnetite (Fig. 3a, b). The stage I quartz (Q1) is a pre-ore stage and is not associated with gold mineralization. (2) The quartz-pyrite stage is characterized by veins containing coarse-grained quartz and pyrite, sericite, chlorite, with minor chalcopyrite, and native gold. The stage II quartz (Q2), the most abundant mineral, mainly appears as euhedral-subhedral grains and is milky to gray in color (Fig. 3c, d). (3) The quartz-gold-polymetallic sulfide stage is characterized by the widespread occurrence of pyrite, chalcopyrite, galena, sphalerite, and native gold, with minor tetrahedrite, chalcocite, electrum, and petzite (Fig. 3e–i). Native gold is locally present along the boundaries or in the fissures of pyrite grains (Fig. 3i). The stage III (Q3) is commonly dark-gray (smoky) in color and characterized by fine-grained anhedral aggregates (Fig. 3d–f). (4) The quartz-carbonate stage is marked by the appearance of carbonate and quartz with minor pyrite, electrum, and petzite but no gold. These minerals fill the fissures

in early veins or occur in the vugs. Of these stages, Au–Cu mineralization occurred mainly during stages II and III.

Sampling and analytical methods

Sample preparation

The quartz samples for fluid inclusion study were collected from a pyrite-sericite-quartz vein (stage I) at depth 300 m and a pyrite-quartz vein (stage II) at depth 300 m in the no. 9 ore zone and a polysulfide-quartz vein (stage III) at depth 250 m and a galena vein (stage III) at depth 160 m in the no. 10 ore zone. The sulfide samples for the noble gas isotopic and Pb isotopic were also selected from the pyrite-quartz vein and the polysulfide-quartz vein.

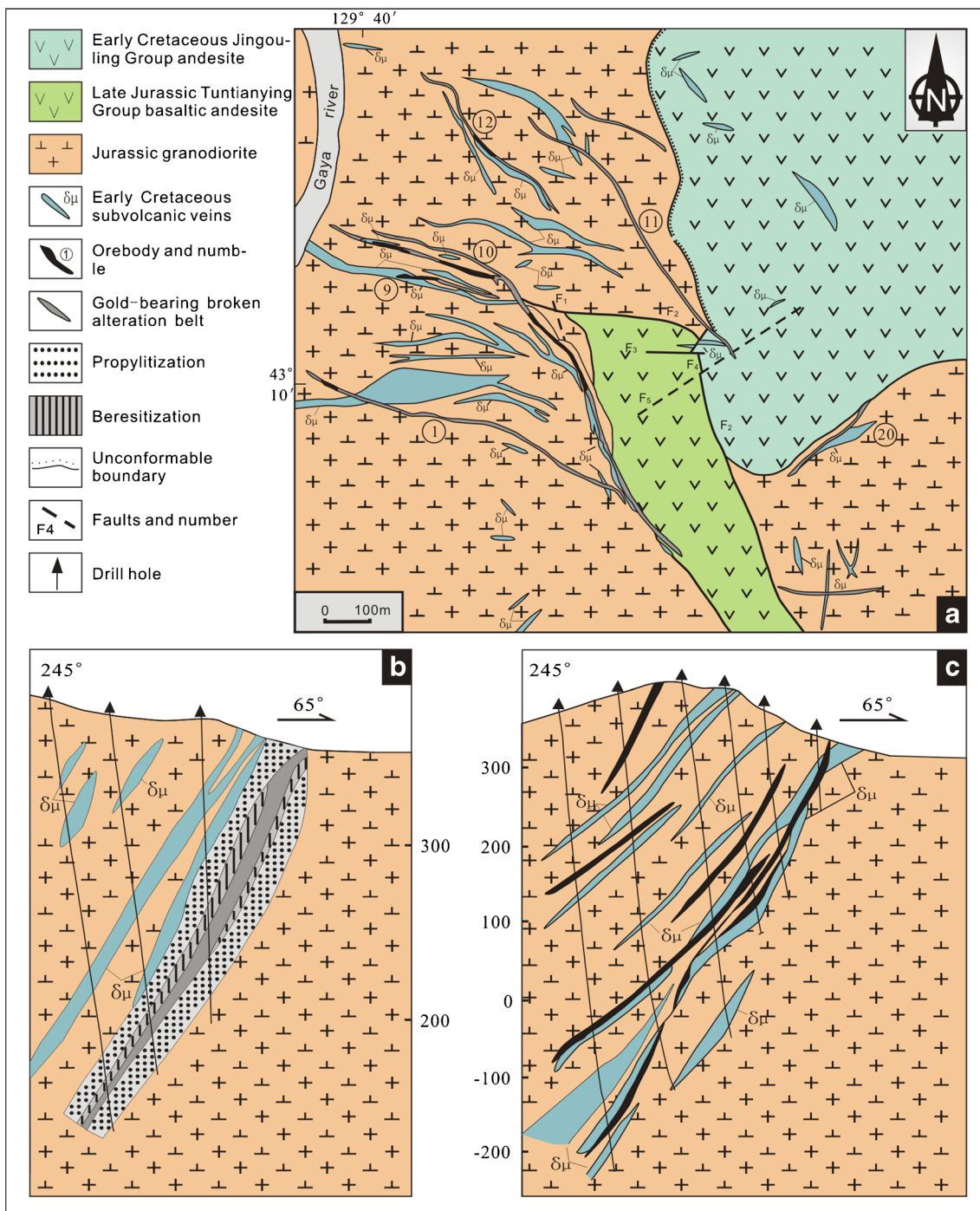


Fig. 2 Geological map of the Naozhi Au–Cu deposit (a) (modified from Cheng et al. 2009). Geological section along exploration line no. 72 (b) and no. 74 (c) (modified from Zhang 2010 and Huang 1997, respectively)

Fluid inclusions in quartz

Forty-one doubly polished thin sections (about 0.20 mm thick) were made for fluid inclusion study, and ten of them were selected to do microthermometric measurement and laser Raman spectroscopic detection.

Microthermometry was performed on a LINKAMTHMS-600 heating/freezing stage at Jilin University, China. Thermocouples were calibrated at -56.6 , 0.0 , and $+374.1$ °C using synthetic fluid inclusions. Measurement precision was approximately ± 0.1 °C on cooling runs and ± 2 °C on heating runs. During testing, the following parameters were applied: if

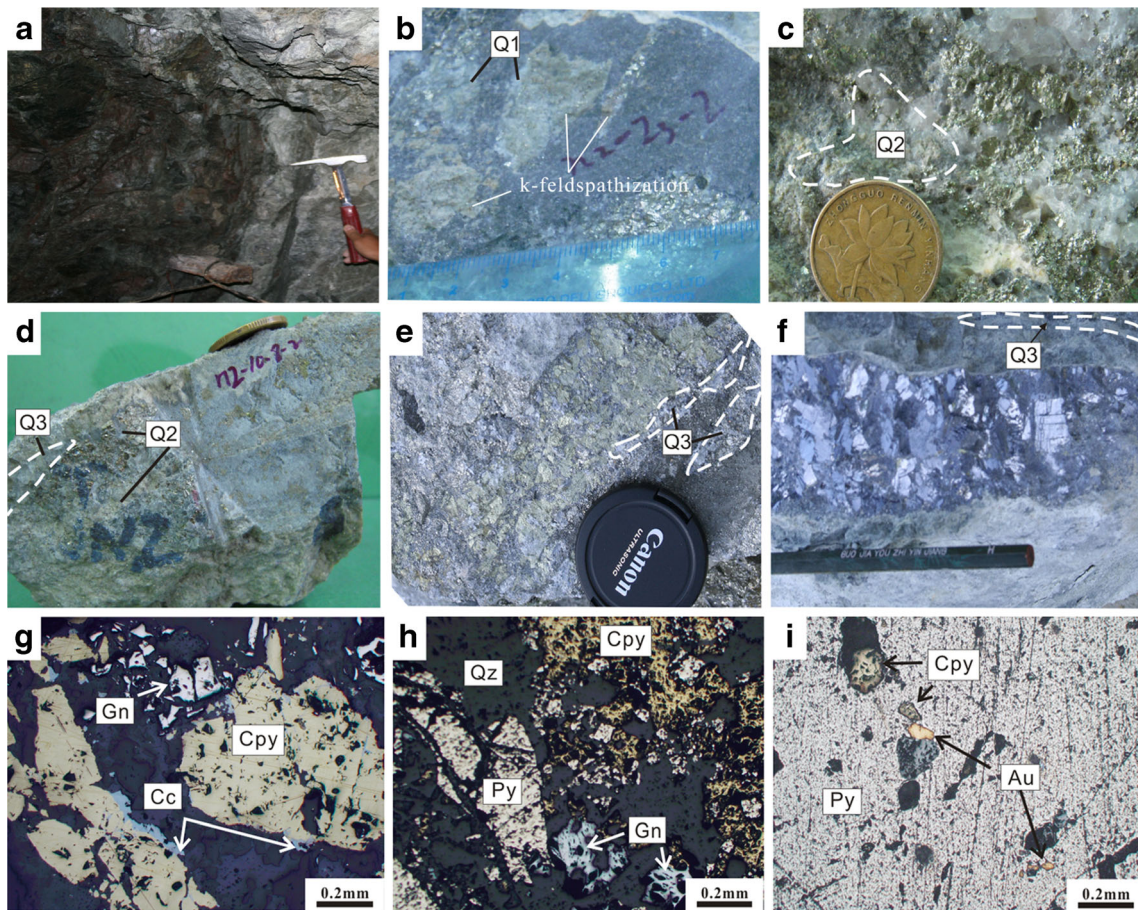
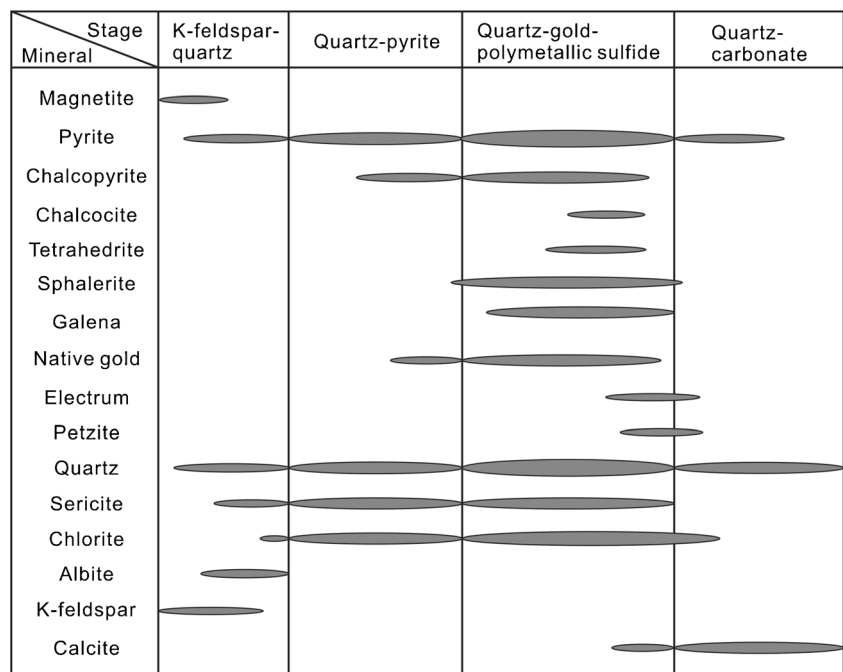


Fig. 3 Hand specimens and micrographs of ore veins in Naozhi Au–Cu deposit. **a** K-feldspar-altered rocks within the mine shaft. **b** Pyrite-sericite-quartz vein showing pyrite-sericite-quartz replaces K-feldspar. **c**, **d** Pyrite-quartz vein. **e** Polymetallic sulfide-quartz veins. **f** Galena veins. **g**

Quartz intergrown with chalcopyrite, galena, and chalcocite. **h** Quartz intergrown with pyrite, chalcopyrite, and galena. **i** Including pyrite and a few of chalcopyrite and native gold. Abbreviations: *Qz* quartz, *Py* pyrite, *Cpy* chalcopyrite, *Cc* chalcocite, *Gn* galena

Fig. 4 Paragenetic sequence of ore and gangue minerals for the Naozhi deposit



the temperature was lower than 30 °C, the heating rate was 1 °C/min; if above 200 °C, the rate was 10 °C min⁻¹; if close to a phase change or around the freezing point, the rate was decreased to <0.2 °C min⁻¹. Salinities of aqueous (NaCl-H₂O) fluid inclusions were calculated using the final melting temperatures of ice points (Bodnar 1993). Salinities of halite-bearing fluid inclusions (FIs) were calculated using the dissolution temperatures of the halite daughter mineral (Hall et al. 1988).

To constrain the fluid inclusion compositions, Raman analysis of 35 single mineral inclusions from the ore samples was carried out with a Renishaw RM2000 at Nanjing University, China, using a 514 AR+ laser with a spot size of 1 μm and a spectral counting time of 10 s. Peak values from the full spectra were obtained at intervals of 1 cm.

Isotopic analysis of noble gases from sulfides

Four pyrite samples and two chalcopyrite samples were crushed to <3 mm. To enable noble gas analysis and to avoid analyzing gases from multistage fluid inclusions (Hu et al. 1998; Burnard et al. 1999; Sumino et al. 2001) great care was taken to select about 2 g of each mineral with homogeneous optical properties and free of fractures.

Noble gas analyses were carried out at the Laboratory for Earthquake Chemistry in Tokyo University, Japan. Noble gases were extracted from each sample in a crushing vessel connected to the gas purification line. The cooled and separated noble gases were analyzed with a VG5400 mass spectrometer (MS-III),

following Nagao et al. 1996 and Matsuda et al. 2002. Analytical errors are less than 10 % (1σ). Blanks for ⁴He, ²⁰Ne, ⁴⁰Ar, ⁸⁴Kr, and ¹³²Xe gave 1.5–4.5 × 10⁻¹¹, 0.8–1.9 × 10⁻¹², 3.8–8.4 × 10⁻¹⁰, 1.7–5.3 × 10⁻¹⁴, and 2.2–9.6 × 10⁻¹⁵ cc standard pressure (STP), respectively. The ³He/⁴He ratio for the helium isotope standard analyzed during the runs was 28.88 ± 0.14 × 10⁻⁵ (HESJ) (Schlosser and Winckler 2002).

Lead isotopic analyses of sulfides

Six samples for Pb isotope analyses of sulfides were performed using a Finnegan Element II type, HR-ICP-MS at the State Key Laboratory of Mineralization, Nanjing University, China. After crushing and sieving the ore samples, the single minerals, with purity of more than 98 %, were picked out under the binocular microscope. Sulfide samples were washed with 0.15 mol/L HCl and high purity water. All of these samples were ground to below 74 μm, and decomposed in the Teflon PFA bottle using HCl and HNO₃. After complete decomposition, they were evaporated to nearly dry and transformed into 0.15 mol/L HCl and 0.65 mol/L HBr medium, then separated in Bio-RadAG 1 × 8 anion exchange column and leached with 1.0 mol/L HNO₃ and heated to dry. Measured Pb isotopic ratios were corrected for instrumental mass fractionation of 0.1 % per atomic mass unit by reference to repeated analyses of the NBS-981 Pb standard. Silicon was the main emitting agent. The prototypes of the Pb isotope ratios were 0.059003 ± 0.000084, 0.91439 ± 0.00017, and 2.16441 ± 0.00097. The blank value for Pb was <1 ng.

Table 1 Characteristics of fluid inclusions in the Naozhi Au–Cu deposit

Inclusion type	Distribution	Shape	Size	Volatile contents	Proportion (%)
Pure gas inclusions (V-type)	Pyrite-sericite-quartz vein and polysulfide-quartz vein	Larger inclusions occur discretely within quartz crystals, whereas small inclusions are clustered and related to healing fractures. These inclusions are monophasic at room temperature.	2–15 μm	–	8
Pure liquid inclusions (L-type)	Galena quartz vein	Individual fluid inclusions are irregularly shaped.	5–15 μm	–	10–15
Gas–liquid two-phase inclusions (W-type)	Extensive development in the sulfide-quartz veins from different stages	The individual fluid inclusions occur as elliptical, negative crystals and are irregular in shape, sometimes necking-down of fluid inclusion can be seen.	3–20 μm	50–80 % (RV)	70–80
CO ₂ -bearing inclusions (C-type)	Pyrite-sericite-quartz vein and pyrite-quartz vein	The C-type inclusions show two or three phases (liquid H ₂ O + liquid CO ₂ ± vapor CO ₂) at room temperature and rounded, elliptical, or negative crystal shapes	Two phases, 8–15 μm; three phases, 15 μm	8–45 % (RL)	5 %
Daughter-mineral-bearing polyphase inclusions (S-type)	Pyrite-sericite-quartz vein	The individual fluid inclusions are semi-elliptical to irregular in shape.	10–20 μm; halite, 2–5 μm; opaque mineral, 0.5–1 μm	–	2

Results and discussion

Properties of ore-forming fluid

Types and characteristics of fluid inclusions

FIs were classified petrographically as follows: isolated FIs and randomly distributed groups of FIs hosted in intragranular quartz crystals were interpreted as primary in origin, and those aligned along micro-fractures in transgranular trails were interpreted as secondary (Roedder 1984; Lu et al. 2004).

Based on composition, phases (L-V-S) at room temperatures and phase transformations during heating and cooling, five fluid inclusion types have been identified (Table 1 and Fig. 5): (1) pure gas inclusions (V-type), (2) pure liquid inclusions (L-type), (3) gas–liquid two-phase inclusions (W-type),

(4) CO₂-bearing inclusions (C-type), and (5) daughter mineral-bearing polyphase inclusions (S-type).

W-type fluid inclusions are the most common FIs in the Naozhi Au–Cu deposit, and they can be further divided into rich-gas inclusions (RV-type) and rich-liquid inclusions (RL-type). The RV-type fluid inclusions are best developed during the early mineralization stage, and the main mineralization stage and the RL-type fluid inclusions occur in Qz of all stages.

Observations under the microscope also recognized necking-down of fluid inclusions in the pyrite-quartz vein (Fig. 5e), suggesting that some of the host quartz and pyrite were locally deformed (Sun et al. 2010). In addition, coexistence of different types of fluid inclusions with very variable liquid/vapor ratios was recognized in the Naozhi samples (Fig. 5a, b), indicating that fluid unmixing might have played

Fig. 5 Microphotographs of typical fluid inclusions in Naozhi Au–Cu deposit. **a** Coexistence of S-type with halite, L-type, and W-type inclusions and **b** coexistence of V-type, C-type, and W-type inclusions in stage I (quartz from pyrite-sericite-quartz vein). **c** C-type inclusion composed of liquid CO₂ and liquid CO₂ and vapor CO₂ in stage II (quartz from pyrite-quartz vein). **d** L-type inclusion composed of liquid H₂O and W-type inclusion in stage III (quartz from galena vein). **e** Necking-down fluid inclusion marked by the red circle in stage II (quartz from pyrite-quartz vein). **f** W-type inclusions composed of vapor H₂O and liquid H₂O in stage III (quartz from polysulfide vein). Abbreviations: *H* halite, *L*_{H₂O} liquid H₂O, *L*_{CO₂} liquid CO₂, *V*_{H₂O} vapor H₂O, *V*_{CO₂} vapor CO₂

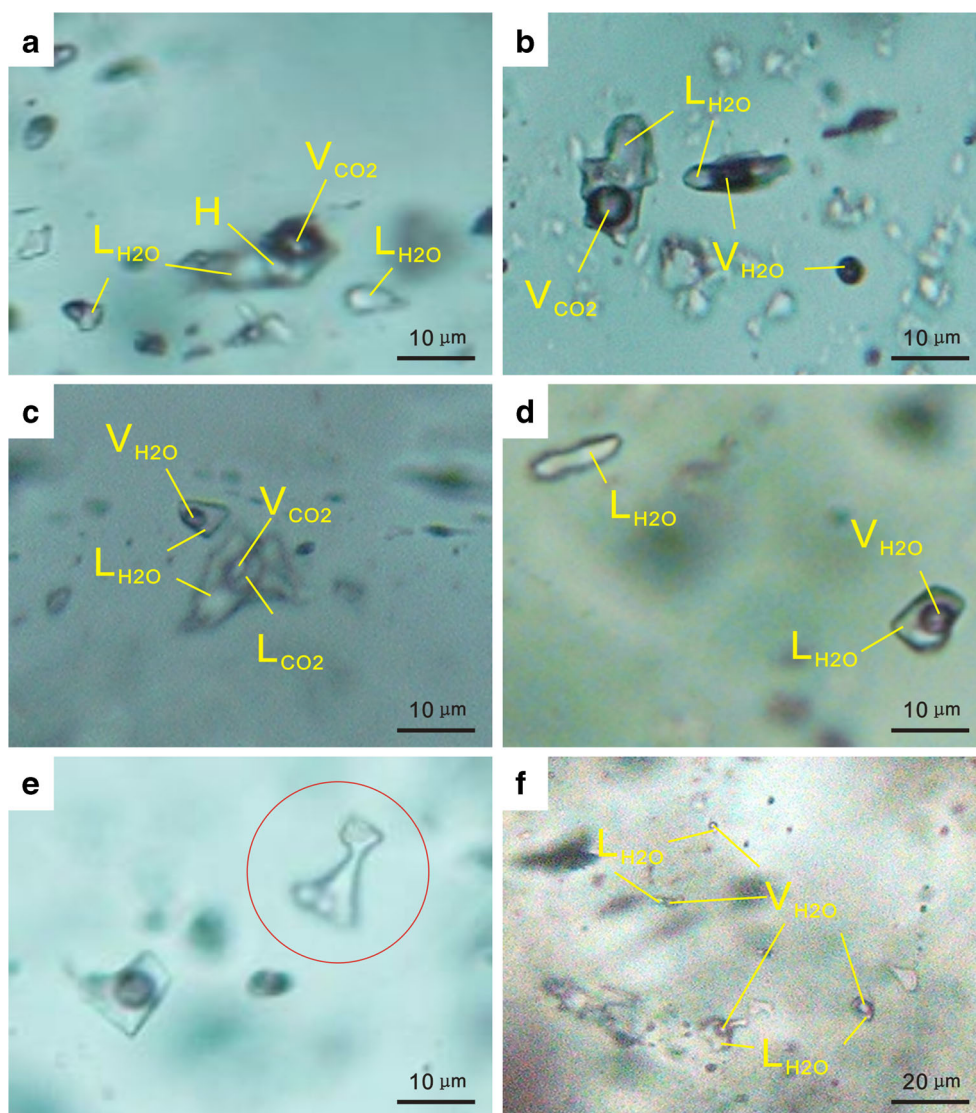


Table 2 Microthermometric data for fluid inclusions of different stage

Stage	Type	Number	$T_{m, ice}$ (°C)	$T_{m, halite}$ (°C)	T_h (°C)	Salinity/wt%
Early (I)	RV	9	-2.7 to -4.4 (3)		335.1–393.5	4.48–7.01
	RL	39	-1.4 to -3.4 (9)		324.7–406.7	2.40–5.55
	HS	3		328.6–400	328.6–400	39.96–46.00
Main (II, III)	RV	13	-1.7 to -5.6 (5)		270–325.4	2.89–8.67
	RL	179	-1.0 to -6.2 (23)		230–338.8	1.73–9.47
			-15.4 to -18 (3)			19.13–21.20
Late (IV)	RV	2	–		195.8–232.2	–
	RL	35	-3.9		154.6–308	6.29

$T_{m, ice}$ temperature of final ice melting, $T_{m, halite}$ final dissolution temperature of halite daughter crystal, T_h total homogenization temperature

an important role during mineralization (Roedder 1984; Li 1988; Lu et al. 2004).

Homogenization temperatures and salinities

The microthermometric dates, summarized in Table 2, were obtained from RV-type, RL-type, and HS-type fluid inclusions of the three hydrothermal stages (Fig. 6). Microthermometric

measurements were not possible for some FIs due to their small sizes.

RV, RL, and HS fluid inclusion types have been recognized in the early hydrothermal stage. Homogenization temperatures are mainly between 335.1 and 393.5 °C, 324.7 and 406.7 °C, and 328.6 and 400 °C, respectively. The $T_{m, ice}$ or $T_{m, halite}$ range from -2.7 to -4.4 °C, -1.4 to -3.4 °C, and 328.6 to 400 °C, respectively, corresponding to a salinity of

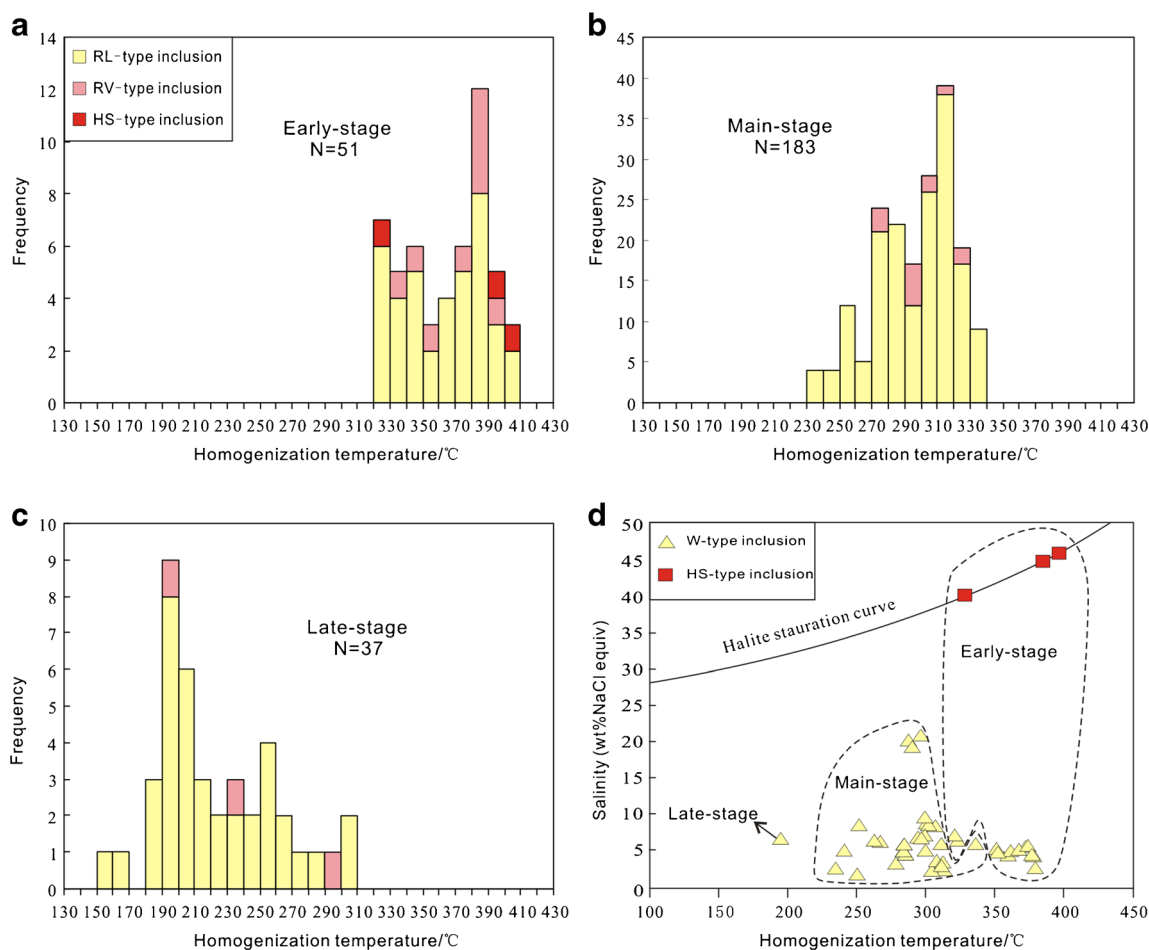


Fig. 6 Histograms of the total homogenization temperatures and salinities of fluid inclusions in different stages

4.48–7.01 wt% NaCl_{eq}, 2.40–5.55 wt% NaCl_{eq}, and 39.96–46.00 wt% NaCl_{eq}.

Quartz crystals from the main hydrothermal stage contain many RV-type and RL-type FIs. The RV-type FIs yield final $T_{m, ice}$ of -1.7 to -5.6 °C and salinities of 2.89–8.67 wt% NaCl_{eq}. These RV-type FIs are homogenized to a liquid phase at temperatures of 270–325.4 °C. The RL-type FIs yielded many $T_{m, ice}$ of -1.0 to -6.2 and three $T_{m, ice}$ of -15.4 to -18 and salinities of 1.73–9.47 wt% NaCl_{eq} and 19.13–21.20 wt% NaCl_{eq}, respectively. Their homogenization temperatures are mainly between 230 and 338.8 °C.

Only RL-type and few RV-type fluid inclusions were observed in the late-stage quartz. Just one $T_{m, ice}$ of -3.9 and salinity of 6.29 wt% NaCl_{eq} was yield in the RL-type FIs. The homogenization temperatures of RL-type and RV-type FIs are 154.6–308 and 195.8–232.2 °C, respectively.

Vapor composition of fluid inclusions

Raman analysis results reveal that the gas compositions of gas-liquid two-phase inclusions of the early mineralization stage

(chlorite-bearing brecciated pyrite quartz vein) are predominantly CO₂ and H₂O (Fig. 7a, b). The gas compositions of gas-liquid two-phase inclusions of the main mineralization stage (chalcopyrite-pyrite quartz vein) are mainly H₂O and minor CO₂ (Fig. 7c, d), and the gas compositions of gas-liquid two-phase inclusions of the late main mineralization stage (quartz from the galena vein) are mainly H₂O (Fig. 7e, f). From these data, it is apparent that the early ore-forming fluids which consisted of CO₂ and H₂O, with H₂O gradually increasing and CO₂ being absent at the late mineralization stage, show that the ore-forming fluid was derived from deep magma degassing and volcanic hydrothermal activity. The H-O isotopic characteristics of fluid inclusions in quartz indicate that the $\delta^{18}O_{H_2O}$ and δD_{V-SMOW} of the early mineralization stage are $+5.87$ and -94% , respectively, and the $\delta^{18}O_{H_2O}$ and δD_{V-SMOW} of the main mineralization stage are -4.7 to $+4.7\%$ and -123.8 to -84.6% , respectively (Feng 1994; Huang 1997; Yang et al. 2010; Table 3). typical of magmatic hydrothermal settings. In the plot of δD vs. $\delta^{18}O_{H_2O}$ (Fig. 8), quartz samples plot near the lower left of the magmatic water field. This may reflect the increasing influence of meteoric water during the evolution of the ore-forming fluid.

Fig. 7 Representative laser Raman spectra of fluid inclusions. **a, b** Vapor phase of W-type inclusions are predominantly CO₂ and H₂O in the early mineralization stage (quartz from pyrite-sericite-quartz vein). **c, d** Vapor phase of W-type inclusions dominated by H₂O and minor CO₂ in the main mineralization stage (quartz from chalcopyrite-pyrite quartz vein). **e, f** Vapor H₂O in W-type inclusion in the late main mineralization stage (quartz from the galena vein)

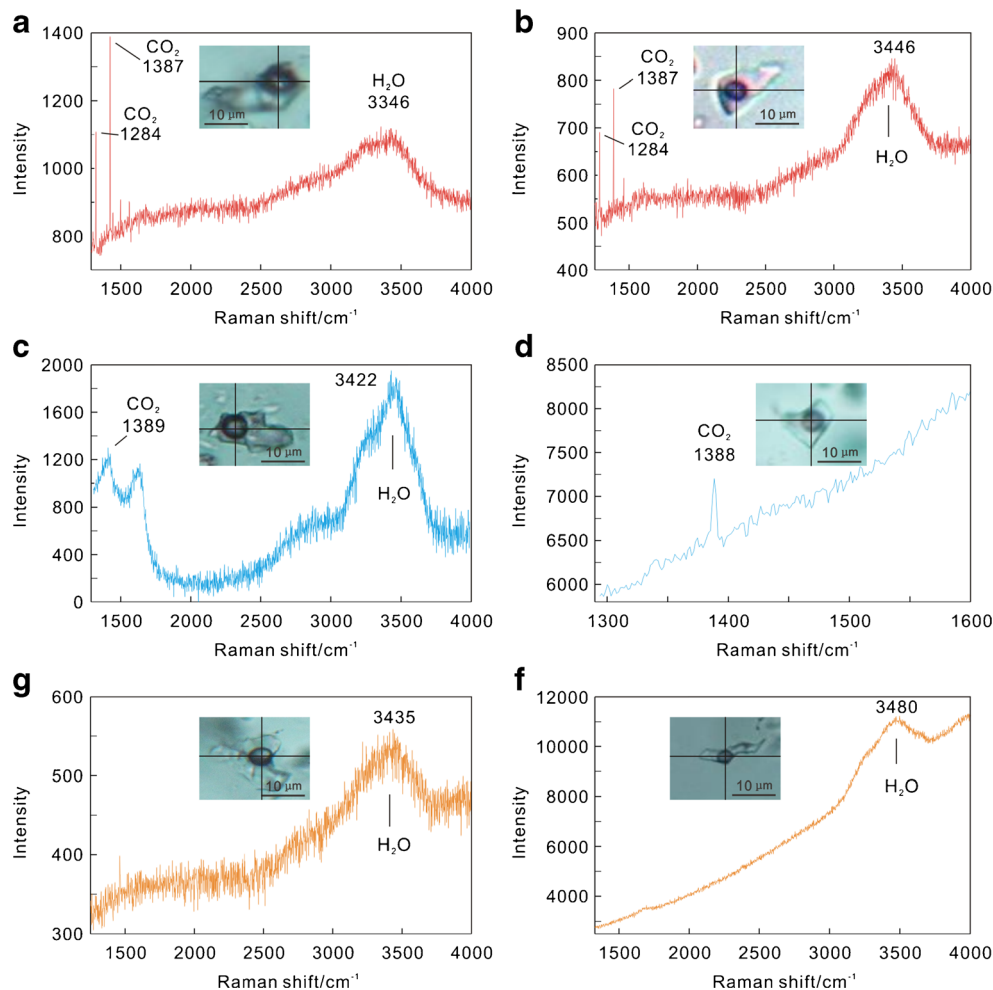


Table 3 Compositions of H-O isotope of fluid inclusions (10^{-3})

Stage	Sample	Test subject	$\delta^{18}\text{O}_\text{Q}$	$\delta^{18}\text{O}_{\text{H}_2\text{O}}$	$\delta\text{D}_{\text{V-SMOW}}$	$\delta^{13}\text{C}_{\text{PDB}}$	T_{h} (°C)	Reference
Early	–	Quartz		+5.87	–94		350	Feng (1994)
Main	–	Quartz (4)	+9.9 ~ +10.5	+3.61 ~ +4.6	–90 ~ –99		318–330	Yang et al. (2010)
	NB124-1	Quartz	+4.6	–1.4	–123.8		327	Huang (1997)
	NB601	Quartz	+10.7	+4.7	–113.1		327	
	NB123	Quartz	+7.5	+0.6	–97.0		298	
	NB417	Quartz	+8.6	+0.2	–84.6		263	
	NB119	Quartz	+4.6	–4.7	–90.6		243	

Noble gas isotopes

Hydrothermal fluids contain noble gases from four ultimate sources (Burnard et al. 1999; Ballentine and Burgess 2002). (1) air-saturated water (i.e., meteoric water, sea water): Air-saturated water has He and Ar isotopic compositions of $^3\text{He}/^4\text{He}=1\text{Ra}$ (where Ra is the $^3\text{He}/^4\text{He}$ value of air, 1.399×10^{-6}) and $^{40}\text{Ar}/^{36}\text{Ar}=295.5$, similar to the atmospheric values because air-saturated water is isotopically in equilibrium with the atmosphere. (2) Mantle-derived fluids: The upper oceanic mantle has $^3\text{He}/^4\text{He}$ ratio of 7–9 Ra, and the subcontinental lithospheric mantle (SCLM) has $^3\text{He}/^4\text{He}$ ratio of 6–8 Ra. Mantle-derived Ar has $^{40}\text{Ar}/^{36}\text{Ar}$ ratios >40,000 (Porcelli et al. 1992; Patterson et al. 1994; Dunai and Baur 1995; Reid and Graham 1996; Gautheron and Moreira 2002) (3) He and Ar produced in the crust. Th and K in crust can produce abundant radiogenic and nucleogenic ^{40}Ar and ^4He . As a result, fluids reacted with crustal rocks will eventually have He and Ar isotopic compositions similar to that of the crust that has $^{40}\text{Ar}/^{36}\text{Ar}$ ratios of 1,000 (Drescher et al. 1998) and $^3\text{He}/^4\text{He}$ ratios of 0.01–0.05 Ra (Stuart et al. 1995).

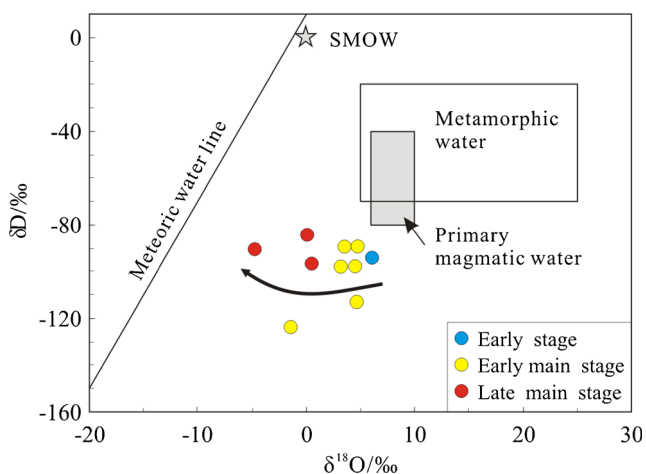


Fig. 8 δD vs. $\delta^{18}\text{O}_{\text{H}_2\text{O}}$ plot in the Naozhi Au–Cu deposit (after Taylor 1997). Data are from Feng (1994), Bing et al. (1995), Huang (1997), and Yang et al. (2010), indicating the evolution of the hydrothermal fluids

Diffusion–fractionation effect of noble gas isotopes in fluid inclusions that is caused by physical properties of host minerals has been concerned by geochemists for a long time (Turner and Stuart 1992; Baptiste and Fouquet 1996; Hu et al. 1998; Mao et al. 2003; Sun et al. 2006). In general, physical diffusion of He isotopes occurs most easily. Olivine and sulfides have good sealing ability, and among the sulfides, pyrite has the highest sealing ability and very low diffusion coefficient (Matsuda et al. 2002).

The values of He in fluid inclusions from pyrite and chalcopyrite vary significantly between 272×10^{-9} and 839×10^{-9} cc STP/g (averaging 529×10^{-9} cc STP/g), ^{20}Ne values are $0.512\text{--}0.857 \times 10^{-9}$ cc STP/g (averaging 0.646×10^{-9} cc STP/g), ^{40}Ar values are $187\text{--}477 \times 10^{-9}$ cc STP/g (averaging 308×10^{-9} cc STP/g), ^{84}Kr values are $13.5\text{--}38.4 \times 10^{-12}$ cc STP/g, and ^{132}Xe values are $1.01\text{--}4.74 \times 10^{-12}$ cc STP/g (Table 4). Noble gas contents are shown in Fig. 9. ^4He , ^{20}Ne , ^{40}Ar , ^{84}Kr , and ^{132}Xe show normal distributions, indicating that these fluid inclusions have suffered no obvious loss of noble gas during analysis and the chalcopyrite also has well-sealing ability.

Atmospheric He contribution can be determined from the $F^4\text{He}$ values, which are defined as the $^4\text{He}/^{36}\text{Ar}$ ratio of the sample relative to the atmospheric $^4\text{He}/^{36}\text{Ar}$ value of 0.1655. A sample containing 100 % atmospheric He has an F value of unity (Kendrick et al. 2001; Zhai et al. 2006; Zeng et al. 2014). The values of $F^4\text{He}$ vary from 3,173 to 4,838, which are 3,000 times higher than in the atmosphere and 15,000 times higher than in air-saturated water (0.18–0.28), indicating that He contribution from the atmosphere was negligible, both before and after the inclusions.

The radiogenic $^{40}\text{Ar}^*$ in geologic samples can be calculated using the formula in Table 4 (Schlosser and Winckler 2002). The contents of radiogenic $^{40}\text{Ar}^*$ vary from 8.8 to 15.5 %, and the contribution of atmospheric ^{40}Ar is 84.5–91.2 %. The values of He in fluid inclusions show that the radiogenic $^{40}\text{Ar}^*$ contents are not mantle-derived but are from crustal sources. Crustal Ar mainly occurs in potassium-bearing micas and K-feldspar (Mcdougall and Harrison 1989). However, as

Table 4 Contents and ratios of noble gas isotopes in the Naozhi Au–Cu deposit

Sample	Mineral	Weight (mg)	³ He/ ⁴ He (Re/Ra) (±1σ)	²⁰ Ne/ ²² Ne (±1σ)	²¹ Ne/ ²² Ne (±1σ)	³⁸ Ar/ ³⁶ Ar (±1σ)
03Jnz-4a	Pyrite	441.4	0.033 ±0.009	9.913 ±0.067	0.0294 ±0.0011	0.18718 ±0.00040
03Jnz-4b	Chalcopyrite	304.3	0.040 ±0.009	9.897 ±0.076	0.0292 ±0.0010	0.18735 ±0.00046
03Jnz-4c	Chalcopyrite	322.1	0.103 ±0.011	9.817 ±0.078	0.0291 ±0.0011	0.18725 ±0.00046
03Jnz-4d	Pyrite	342.5	0.037 ±0.007	9.897 ±0.070	0.0290 ±0.0010	0.18742 ±0.00056
Jnz-9a	Pyrite	346.1	0.104 ±0.013	9.874 ±0.096	0.0295 ±0.0010	0.18761 ±0.00062
Jnz-9b	Pyrite	373.4	0.050 ±0.007	9.960 ±0.074	0.0295 ±0.0012	0.18731 ±0.00038
Air				9.8		0.188

Sample	⁴⁰ Ar/ ³⁶ Ar (±1σ)	⁴ He (10 ⁻⁹ cc STP/g)	²⁰ Ne	⁴⁰ Ar	⁸⁴ KE (10 ⁻¹² cc STP/g)	¹³² Xe	⁴⁰ Ar*%o	⁴⁰ Ar*/ ⁴ He	F ⁴ He
03Jnz-4a	341.1 ±0.8	438	0.599	284	21.8	1.92	13.4	0.031	3,173
03Jnz-4b	349.7 ±0.7	839	0.857	477	38.4	4.74	15.5	0.018	3,713
03Jnz-4c	347.4 ±0.9	272	0.720	359	33.9	3.73	14.9	0.055	1,589
03Jnz-4d	347.7 ±1.0	593	0.512	257	20.7	1.76	15.0	0.025	4,838
Jnz-9a	324.1 ±0.8	436	0.561	187	13.5	1.01	8.8	0.020	4,563
Jnz-9b	339.2 ±0.7	595	0.666	285	19.4	1.75	12.9	0.022	4,275
Air	295.5								

³He_{DM}/³He_m = ((1 - (³He/⁴He)_c) / (³He/⁴He)_m) / (1 - (³He/⁴He)_c) / (³He/⁴He)_{DM}) × 100; ²⁰Ne_{DM}/²⁰Ne_m = ((1 - (³He/⁴He)_{air}) / (³He/⁴He)_m) / (1 - (²⁰Ne/²²Ne)_{air}) / (²⁰Ne/²²Ne)_{DM}) × 100; Ar%o = ((⁴⁰Ar/³⁶Ar)_m - 295.5) / (⁴⁰Ar/³⁶Ar)_m × 100; F⁴He = (⁴He/³⁶Ar)_m / (⁴He/³⁶Ar)_{air}. After refs. (Schlosser and Winckler 2002; Ballentine and Burgess 2002)

DM the mantle, m observed value, c crustal fluid, air atmosphere air

the measured samples are fluid inclusions from sulfides being devoid of K and the time of entrapment is Early Cretaceous (Han et al. 2013) it can be assumed that these values represent those of the fluid at the time of inclusion entrapment.

In terms of isotope ratios, the ³He/⁴He ratios cover the range 0.033 to 0.104 Ra with an average of 0.061 Ra. These values are far below the He isotopic composition of the upper mantle (6–8 Ra) and the atmosphere (1 Ra) (Allègre et al. 1987; Sarda et al. 1988; Porcelli et al. 1992; Patterson et al.

1994; Dunai and Baur 1995) but close to the composition of fluid in young continental crust (0.01–0.05 Ra) (Stuart et al. 1995). The ²⁰Ne/²²Ne and ²¹Ne/²²Ne ratios are in the range of 9.817–9.960 and 0.0290–0.0295, respectively, which is similar to the composition of the atmosphere ([²⁰Ne/²²Ne]_a = 9.8, [²¹Ne/²²Ne]_a = 0.29). The ³⁸Ar/³⁶Ar and ⁴⁰Ar/³⁶Ar ratios are in the range of 0.18718–0.18761 and 324–349, respectively. The ³⁸Ar/³⁶Ar ratios are consistent with the ratio of air-saturated water (0.188), whereas the ⁴⁰Ar/³⁶Ar ratios are slightly higher than the ratio of air-saturated water (295.5) and young continental crust fluid and are much lower than the value for the mantle (>40,000). The ⁴⁰Ar*/⁴He ratios are 0.018–0.055, far below the ratios of crustal rocks (0.2) and continental lithospheric mantle (0.5) (Ballentine and Burgess 2002). Figure 10a shows ⁴He contents vs. ³He/⁴He ratios. All of the compositional points fall in the range of crustal fluid or between the crustal fluid and mantle fluid on the right side of the cutoff line. This indicates that the fluid inclusions from minerals in this deposit have relatively high radiogenic ⁴He and are dominated by crustal components (Gautheron et al. 2005). On the diagram of ⁴He vs. ³He/⁴He (Fig. 10a) and ⁴⁰Ar*/⁴He vs. ³He/⁴He (Fig. 10b), all the compositional points lie in or near the range of crustal fluid, indicating the ore-forming fluids of Naozhi Au–Cu deposit widely hold the properties of young crustal fluid, which is significantly different from the noble gas isotopic components of Xiaoxinancha Au-rich Cu deposit (Sun et al. 2008c).

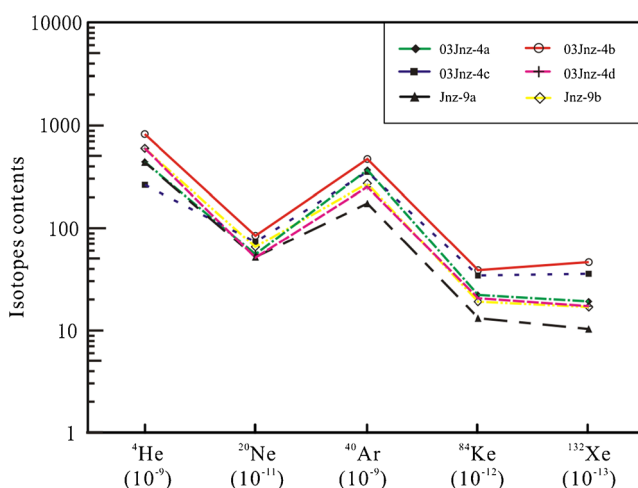


Fig. 9 Noble gas contents of fluid inclusions in the ore minerals

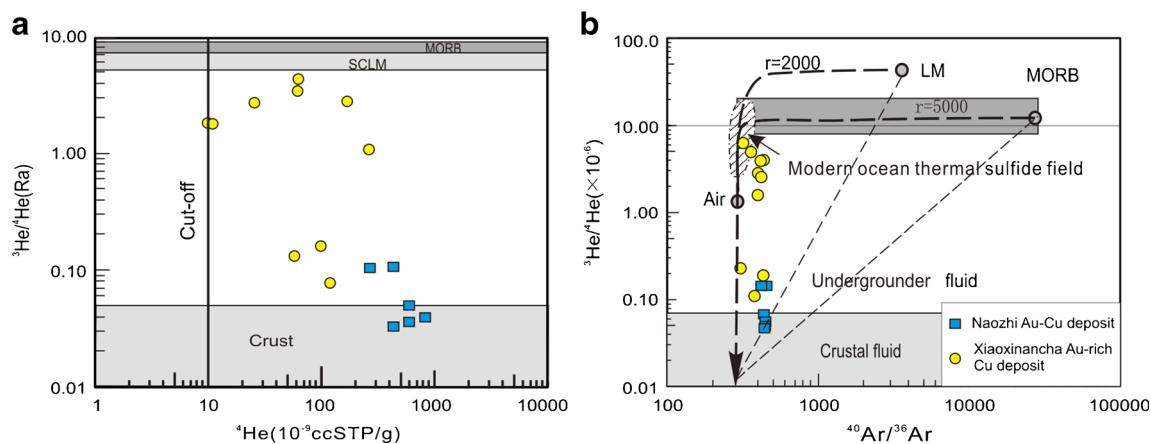


Fig. 10 Plot of **a** ^4He vs. $^3\text{He}/^4\text{He}$ (after Gautheron et al. 2005; Ballentine and Burgess 2002) and **b** $^3\text{He}/^4\text{He}$ vs. $^{40}\text{Ar}/^{36}\text{Ar}$ (after Allègre et al. 1987; O’Nions and Tolstikhin 1994; Langmuir et al. 1978) in fluid inclusions

from the Naozhi Au–Cu deposit and Xiaoxinancha Au-rich Cu deposit. Data of Xiaoxinancha Au-rich Cu deposit from Sun et al. (2008c)

Lead isotopic composition of sulfides

The lead isotopic results are given in Table 5. The $^{206}\text{Pb}/^{204}\text{Pb}$, $^{207}\text{Pb}/^{204}\text{Pb}$, and $^{208}\text{Pb}/^{204}\text{Pb}$ ratios of three pyrite samples vary from 18.3392 to 18.3667, 15.5323 to 15.5603, and 38.1595 to 38.2508, respectively. The $^{206}\text{Pb}/^{204}\text{Pb}$, $^{207}\text{Pb}/^{204}\text{Pb}$, and $^{208}\text{Pb}/^{204}\text{Pb}$ ratios of three chalcopyrite samples vary from 18.1822 to 18.3979, 15.5215 to 15.5998, and 38.1313 to 38.3786, respectively. The lead isotope compositions are similar to those of sulfides in the Xiaoxinancha gold-rich porphyry copper deposit (Men et al. 2011) which show that the data fall in the fields between MORB and a young lower crust source (Fig. 11a), or on the line representing the evolution of young orogenic belts (Fig. 11b). As mentioned above, the deposit has been dated between 130 and 123 Ma (Meng et al. 2001; Han et al. 2013) these values can be assumed to be close to their initial ratios.

Genetic types of deposit

Our results show that polysulfide-quartz vein ores make up the main ore body in the Naozhi Au–Cu deposit. Wall rock alteration includes silicification, sericitization, chloritization, and minor carbonatization and argillization. Mineralization types

are mainly pyrite and chalcopyrite, followed by galena, sphalerite, bornite, chalcocite, and natural gold, electrum, and petzite. Mineralization occurred through four stages: a pyrite-sericite-quartz stage, a pyrite-quartz vein stage, a quartz-gold-polymetallic sulfide stage, and a calcite-quartz stage. The homogenization temperatures and salinities of these main mineralization stages were in the range of 230–338.8 °C and 1.73–9.47 wt% NaCl_{eq} , respectively; oxidation–reduction reactions (chalcopyrite \rightarrow bornite + chalcocite) occurred during mineralization. On the basis of the mineralization–alteration features and low fluid inclusion salinity, the deposit is best described as a medium-temperature magmatic hydrothermal deposit or a medium-sulfidation epithermal deposit (Mao et al. 2007; Sillitoe 2008). Likewise, the Naozhi Au–Cu deposit is analogous to the Jinchanggouliang epithermal Au–Cu deposit (122 Ma, Mao et al. 2007) of the Chifeng area and to the Erdaogou epithermal Au–Cu deposit (126 ± 1 Ma, Miao et al. 2003) of western Liaoning in terms of its geological features, fluid inclusion compositions, and formation age (Chen et al. 2005; Miao et al. 2003). This indicates that this stage of mineralization occurred during Early Cretaceous volcanism associated with an extensional system within the Xing’an–Mongolian orogenic belt, a magmatic arc system related to positive subduction of the Pacific Plate

Table 5 Pb isotope date of ore minerals in the Naozhi Au–Cu deposit

Sample	Name	Test subject	$^{206}\text{Pb}/^{204}\text{Pb}$	2σ	$^{207}\text{Pb}/^{204}\text{Pb}$	2σ	$^{208}\text{Pb}/^{204}\text{Pb}$	2σ
03Jnz-4a	Quartz-gold-polymetallic sulfide vein	Pyrite	18.3628	8	15.5570	7	38.2396	16
03Jnz-4b	Quartz-gold-polymetallic sulfide vein	Chalcopyrite	18.3587	2	15.5448	1	38.1986	28
Jnz-9a	Quartz-gold-polymetallic sulfide vein	Pyrite	18.3392	9	15.5323	8	38.1595	19
Jnz-9b	Quartz-gold-polymetallic sulfide vein	Chalcopyrite	18.1822	3	15.5215	9	38.1313	22
03Jnz6	Pyrite-quartz vein	Pyrite	18.3667	9	15.5603	10	38.2508	32
03Jnz6-a	Pyrite-quartz vein	Chalcopyrite	18.3979	10	15.5998	13	38.3786	43

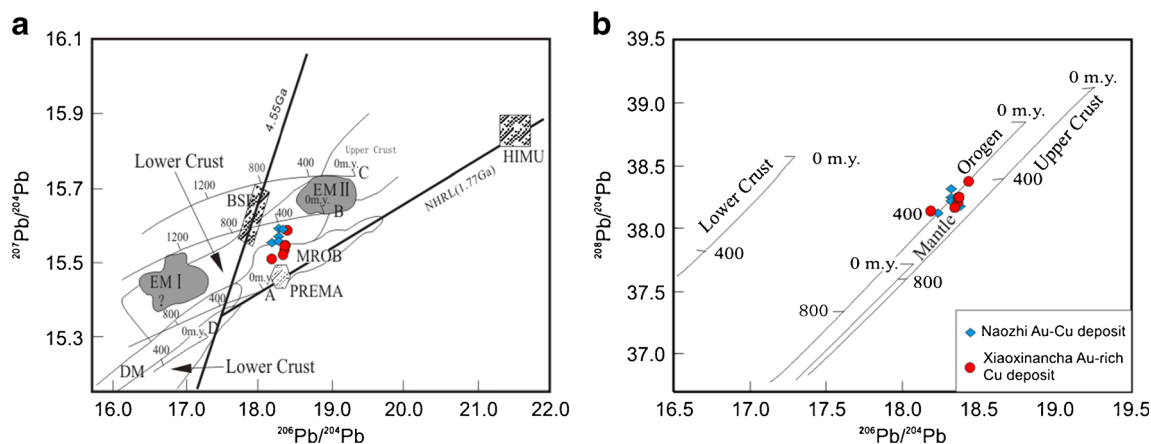


Fig. 11 $^{207}\text{Pb}/^{204}\text{Pb}$ vs. $^{206}\text{Pb}/^{204}\text{Pb}$ diagram (a) and $^{208}\text{Pb}/^{204}\text{Pb}$ vs. $^{206}\text{Pb}/^{204}\text{Pb}$ diagram (b) of sulfides from the Naozhi Au–Cu deposit (after Zartman and Doe 1981). Data of Xiaoxinancha Au-rich Cu deposit are from Men et al. (2011)

underneath the Eurasian Plate, and the ore-forming components were brought to shallow crust by molten magma or supercritical fluid and so on (Sillitoe 1997). The metallogenesis in this area is closely related to high-K calc-alkaline intermediate-acid granitic and porphyritic pyroxene diorite magmatism (Chen et al. 2005; Mao et al. 2007).

Combined with the characteristics of diorite veins closely associated with mineralization ($(^{87}\text{Sr}/^{86}\text{Sr})_I=0.705024-0.704975$, $\text{Nd}(t)=+2.60$ to $+2.69$, $T_{\text{DM}2}=856-863$ Ma, our unpublished data) in the Naozhi deposit, we further conclude that the magma was derived from partial melting of lower continental crust with residual ocean property, produced during the subduction of Pacific plate. Mineralizing fluids exsolved during the late crystallization phase and were strongly contaminated by crustal materials/fluids during ascent, including meteoric water. The mixed ore-forming fluids migrated to the secondary brittle structures in the shear zone and finally precipitated auriferous sulfide-quartz ores because of decline of temperature and pressure of the ore-forming fluids.

Conclusions

Through systematic research of ore geology, microscopic feature, components and rare gases, isotopic components of fluid inclusion, and lead isotopic components of sulfides, we can make further conclusions as follows:

1. The Naozhi deposit is a predominantly sulfide-quartz vein Au–Cu gold deposit, formed through four stages: a K-feldspar stage, a pyrite-quartz vein stage, a quartz-gold-polymetallic sulfide stage, and a calcite-quartz vein stage. Fluid inclusions are mainly gas–liquid two-phase inclusions (W), followed by pure gas inclusions (V), pure liquid inclusions (L), CO_2 -bearing inclusions (C), and rare daughter mineral-bearing polyphase inclusions (S).

2. The initial ore-forming fluid of Naozhi Cu–Au gold deposit is $\text{CO}_2\text{-H}_2\text{O-NaCl}$ ore-bearing fluid with medium–high temperature and low salinity. The mineralizing fluid is not homogeneous from the early stage to the late stage and occurs boiling during the early stage and main ore-forming stage, which result in precipitating of ore-forming elements.
3. Combined with stable isotope data and the chronology of diagenesis and metallogenesis, our new data suggest that the ore-forming fluids originated from melting of the lower crust, produced during the subduction of an oceanic slab. Mineralizing fluids exsolved during the late crystallization phase and were strongly contaminated by crustal materials/fluids during ascent, including meteoric water. Mineral precipitation occurred at a shallow crustal level.

Acknowledgments The authors thank Prof. I. Kaneoka, Drs. A. Shmizu and N. Ebisawa (Laboratory for Earthquake Chemistry, Graduate School of Science, University of Tokyo) and Prof. Lai Yong (Peking University) for their support during the fluid inclusion noble gas experiments, and the staff of the State Key Laboratory of Mineralization, Nanjing University and the Geological Fluid Laboratory, Jilin University for help with measuring the temperature and composition of fluid inclusions. In particular, we thank two reviewers for their critical reviews and suggestions that improved the manuscript. This work was funded by the National Natural Science Foundation of China (Grant Nos. 40772052 and 41172072), the major project for the National Natural Science Foundation of China (Grant No. 41390444), the Project for Scientific and Technology Development (Grant No. 20100450), the Chinese Geological Survey Programme (Grant No. [2010]26-06), and the Geological Survey of Heilongjiang Province (Grant No. 3R1101604422).

References

- Allège CJ, Staudacher T, Sarda P (1987) Rare gas systematics: formation of the atmosphere, evolution and structure of the Earth's mantle. *Earth Planet Sci Lett* 81:127–150. doi:10.1016/0012-821X(87)90151-8

- Ballentine CJ, Burgess R (2002) Tracing fluid origin, transport and interaction in the crust. *Rev Mineral Geochem* 47:539–614. doi:10.2138/mg.2002.47.13
- Baptiste PJ, Fouquet Y (1996) Abundance and isotopic composition of helium in hydrothermal sulfides from the East Pacific Rise at 13°N. *Geochim Cosmochim Acta* 60:87–93. doi:10.1016/0016-7037(95)00357-6
- Bing ZY, Zhang HT, Wang LS, Chen RY (1995) The multiple metallogenic model of the porphy-epithermal copper-gold deposits, in Eastern Jilin and Heilongjiang. *Mineral Deposits* 14:174–183 (in Chinese with English abstract)
- Bodnar RJ (1993) Revised equation and table for determining the freezing point depression of H₂O-NaCl solutions. *Geochim Cosmochim Acta* 57:683–684. doi:10.1016/0016-7037(93)90378-A
- Burnard PG, Hu RZ, Turner G, Bi XW (1999) Mantle, crustal and atmospheric noble gases in Ailaoshan Gold deposits, Yunnan Province, China. *Geochim Cosmochim Acta* 63:1595–1604. doi:10.1016/S0016-7037(99)00108-8
- Chai P, Sun JG, Xing SW, Men LJ, Han JL (2015) Early Cretaceous arc magmatism and high-sulphidation epithermal porphyry Cu–Au mineralization in Yanbian area, Northeast China: the Duhuangling example. *Int Geol Rev* 57:1267–1293. doi:10.1080/00206814.2014.960013
- Chen JQ, Sun JG, Piao SC, Zhao JK, Zhai YF (2005) Genesis and significance of dark dikes in the Jinchanggouliang mine area, Inner Mongolia: evidences from geochemistry of the major and trace elements. *J Jilin Univ (Earth Sci Ed)* 35:707–713 (in Chinese with English abstract)
- Cheng MH, Xue XY, Li WL (2009) Geologic characteristics of volcanic-type gold deposit in Wangqing County, Naozhi. *Jilin Geol* 28:25–27 (in Chinese with English abstract)
- Cooke DR, Simmons SF (2000) Characteristics and genesis of epithermal gold deposits. *Rev Econ Geol* 13:221–244
- Drescher J, Kirsten T, Schäfer K (1998) The rare gas inventory of the continental crust, recovered by the KTB Continental Deep Drilling Project. *Earth Planet Sci Lett* 154:247–263. doi:10.1016/S0012-821X(97)00185-4
- Dunai TJ, Baur H (1995) Helium, neon and argon systematics of the European subcontinental mantle: implications for its geochemical evolution. *Geochim Cosmochim Acta* 59:2767–2783. doi:10.1016/0016-7037(95)00172-V
- Feng SZ (1994) Geological characteristics and metallogenic model of Naozhi gold deposit, in Wangqing. *Gold Geol* 39:23–26 (in Chinese)
- Gautheron C, Moreira M (2002) Helium signature of the subcontinental lithospheric mantle. *Earth Planet Sci Lett* 199:39–47. doi:10.1016/S0012-821X(02)00563-0
- Gautheron C, Moreira M, Allègre C (2005) He, Ne and Ar composition of the European lithospheric mantle. *Chem Geol* 217:97–112. doi:10.1016/j.chemgeo.2004.12.009
- Groves DI, Bierlein FP (2007) Geodynamic settings of mineral deposit systems. *J Geol Soc Lond* 164:19–30. doi:10.1144/0016-76492006-065
- Hall DL, Sterner SM, Bodnar R (1988) Freezing point depression of NaCl-KCl-H₂O solutions. *Econ Geol* 83:197–202. doi:10.2113/gsecongeo.83.1.197
- Han SJ, Sun JG, Bai LA, Xing SW, Chai P, Zhang Y, Yang F, Meng LJ, Li YX (2013) Geology and ages of porphyry and medium- to high-sulphidation epithermal gold deposits of the continental margin of Northeast China. *Int Geol Rev* 55:287–310. doi:10.1080/00206814.2012.695472
- Hedenquist JW, Lowenstern JB (1994) The role of magmas in the formation of hydrothermal ore deposits. *Nature* 370:519–527. doi:10.1038/370519a0
- Hu RZ, Burnard PG, Turner G, Bi XW (1998) Helium and argon isotope systematics in fluid inclusions of Machangqing copper deposit in west Yunnan province, China. *Chem Geol* 146:55–63. doi:10.1016/S0009-2541(98)00003-5
- Huang GC (1997) Discussion on genetic relation between the Naozhi gold deposit and the Mesozoic volcanic rock series in Naozhi, Jilin province. *Miner Resour Geol* 11:32–38 (in Chinese with English abstract)
- Jiang SH, Nie FJ, Zhang Y, Hu P (2004) The latest advances in the research of epithermal deposits. *Earth Science Front* 11:401–411 (in Chinese with English abstract)
- Jin K (2003) Petrology and geochemistry of Mesozoic volcanic rocks in Yanbian area: constraints on transformation of tectonic system and composition of lithosphere. Ph.D. thesis, Jilin University (in Chinese with English abstract)
- Kendrick MA, Burgess R, Patrick RAD, Turner G (2001) Fluid inclusion noble gas and halogen evidence on the origin of Cu-porphyry mineralizing fluids. *Geochim Cosmochim Acta* 65:2651–2668
- Langmuir CH, Vocke RD, Hanson GN, Hart SR (1978) A general mixing equation with applications to Icelandic basalts. *Earth Planet Sci Lett* 37:380–392. doi:10.1016/0012-821X(78)90053-5
- Li ZL (1988) Experimental geochemistry. Geological Publishing House, Beijing, pp 1–326 (in Chinese)
- Li HN, Yang GB (1991) Geochemical characteristics of the volcanic gold deposits and mineralization in Yanbian Prefecture, Jilin Province. *Gold* 12:6–12 (in Chinese with English abstract)
- Lin BL (2013) Study on the mineralization tectonic setting and genesis of Naozhi gold deposit, eastern Jilin Province. Masters thesis, Jilin University (in Chinese with English abstract)
- Lu HZ, Fan HR, Ni P, Ou GX, Shen K, Zhang WH (2004) Fluid inclusions. Science Press, Beijing, pp 1–487 (in Chinese with English abstract)
- Mao JW, Li YQ, Goldfarb R, He Y, Zaw K (2003) Fluid inclusion and noble gas studies of the Dongping gold deposit, Hebei province, China: a mantle connection for mineralization? *Econ Geol* 98:517–534. doi:10.2113/98.3.517
- Mao JW, Li XF, White NC, Zhao CS, Zhang ZH, Wang YT, Hu HB (2007) Types, characteristics, and geodynamic settings of Mesozoic epithermal gold deposits in eastern China. *Resour Geol* 57:435–454. doi:10.1111/j.1751-3928.2007.00033.x
- Matsuda J, Matsumoto T, Sumino H, Nagao K, Yamamoto J, Miura Y, Kaneoka I, Takahata N, Sano Y (2002) The ³He/⁴He ratio of the new internal He Standard of Japan (HESJ). *Geochem J* 36:191–195. doi:10.2343/geochemj.36.191
- McDougall I, Harrison TM (1989) Geochronology and thermochronology by the ⁴⁰Ar-³⁹Ar method. University Press, Oxford
- Men LJ, Sun JG, Zhang ZJ, Li YX, Xing SW, Cui PL (2011) An isotopic (Sr, Nd and Pb) tracer study on the Xiaoxinancha gold-rich copper deposit in Yanbian, China: implication for the geodynamic model of diagenesis and metallogenesis. *Acta Geol Sin-Engl* 85:175–188. doi:10.1111/j.1755-6724.2011.00388.x
- Meng QL, Zhou YC, Chai SL (2001) The porphy-epithermal veins copper-gold deposits, in Eastern Jilin and Heilongjiang. Jilin Science and Technology Press, Changchun, pp 1–162 (in Chinese with English abstract)
- Miao LC, Fan WM, Zhai MG, Qiu YM, McNaughton NJ, Groves DI (2003) Zircon SHRIMP U-Pb geochronology of the granitoid intrusions from Jinchanggouliang-Erdaogou gold orefield and its significance. *Acta Petrol Sin* 19:71–80
- Nagao K, Ogata N, Miura YN, Yamaguchi K (1996) Ar isotope analysis for K-Ar dating using two modified-VG5400 mass spectrometers-I: isotope dilution method. *J Mass Spectrom Soc Jpn* 44:39–61. doi:10.5702/massspec.44.39
- O’Nions RK, Tolstikhin IN (1994) Behaviour and residence times of lithophile and rare gas tracers in the upper mantle. *Earth Planet Sci Lett* 124:131–138. doi:10.1016/0012-821X(94)00070-0

- Patterson DB, Honda M, McDougall I (1994) Noble gases in mafic phenocrysts and xenoliths from New Zealand. *Geochim Cosmochim Acta* 58:4411–4427. doi:10.1016/0016-7037(94)90344-1
- Peng YJ, Zhao CB (2001) The evolution of the paleo Jihei orogenic belt and accretion of the continental crust. *Jilin Geol* 20:1–9 (in Chinese with English abstract)
- Porcelli DR, O’Nions RK, Galer SJG, Cohen AS, Matthey DP (1992) Isotopic relationships of volatile and lithophile trace elements in continental ultramafic xenoliths. *Contrib Mineral Petrol* 110:528–538. doi:10.1007/BF00344086
- Reid MR, Graham DW (1996) Resolving lithospheric and sub-lithospheric contributions to helium isotope variations in basalts from the southwestern US. *Earth Planet Sci Lett* 144:213–222. doi:10.1016/0012-821X(96)00166-5
- Roedder E (1984) Fluid inclusions. *Rev Mineral* 12:1–644
- Sarda P, Staudacher T, Allègre CJ (1988) Neon isotopes in submarine basalts. *Earth Planet Sci Lett* 91:73–88. doi:10.1016/0012-821X(88)90152-5
- Schlosser P, Winckler G (2002) Noble gases in ocean water and sediments. *Rev Mineral Geochem* 47:701–730. doi:10.2138/rmg.2002.47.15
- Sillitoe RH (1997) Characteristics and controls of the largest porphyry copper-gold and epithermal gold deposits in the circum-Pacific region. *Aust J Earth Sci* 44:373–388. doi:10.1080/08120099708728318
- Sillitoe RH (2008) Special paper: major gold deposits and belts of the North and South American Cordillera: distribution, tectonomagmatic settings, and metallogenic considerations. *Econ Geol* 103:663–687. doi:10.2113/gsecongeo.103.4.663
- Stuart FM, Burnard PG, Taylor RP, Turner G (1995) Resolving mantle and crustal contributions to ancient hydrothermal fluids: He–Ar isotopes in fluid inclusions from Dae Hwa W–Mo mineralisation, South Korea. *Geochim Cosmochim Acta* 59:4663–4673. doi:10.1016/0016-7037(95)00300-2
- Su FX, Wang XY, Jia WG (2003) Study on typomorphic characteristics of pyrite in the Naozhi Gold Deposit, Jilin. *Gold* 24:13–16 (in Chinese with English abstract)
- Sumino H, Nagao K, Notsu K (2001) Highly sensitive and precise measurement of helium isotopes using a mass spectrometer with double collector system. *J Mass Spectrom Soc Jpn* 49:61–68. doi:10.5702/massspec.49.61
- Sun XM, Xu L, Zhai W, Tang Q, Liang YH, Liang JL, Zhang ZM, Shen K (2006) Noble gases isotopic compositions of fluid inclusions in quartz veins and crystals collected from CCSD and Donghai HP–UHP metamorphic rocks. *Acta Petrol Sin* 22:1999–2008
- Sun JG, Chen L, Zhao JK, Men LJ, Feng W, Chen D, Liang SN (2008a) SHRIMP U–Pb dating of zircons from Late Yanshanian granitic complex in Xiaoxinancha gold-rich copper orefield of Yanbian and its geological implications. *Mineral Deposits* 27:319–328 (in Chinese with English abstract)
- Sun JG, Men LJ, Zhao JK, Chen L, Liang SN, Chen D, Feng W (2008b) Zircon chronology of melanocratic dykes in the district of the Xiaoxinancha Au-rich Cu deposit in Yanbian and its geological implication. *Acta Geol Sin-Engl* 82:517–527
- Sun JG, Zhao JK, Chen JQ, Nagao K, Sumino H, Shen K, Men LJ, Chen L (2008c) Ore-forming mechanism for the Xiaoxinancha Au-rich Cu deposit in Yanbian, Jilin Province, China: evidence from noble gas isotope geochemistry of fluid inclusions in minerals. *Sci China Ser D* 51:216–228
- Sun XM, Wei HX, Zhai W, Shi GY, Liang YH, Mo RW, Han MX, Zhang XG (2010) Ore-forming fluid geochemistry and metallogenic mechanism of Bangbu large-scale orogenic gold deposit in southern Tibet, China. *Acta Petrol Sin* 26:1672–1684
- Taylor HP (1997) Oxygen and hydrogen isotope relationships in hydrothermal mineral deposits. In: Barnes HL (ed) *Geochemistry of hydrothermal ore deposits*, 3rd edn. Wiley, New York, pp 229–302
- Turner G, Stuart FM (1992) Helium/heat ratios and deposition temperatures of sulphides from the ocean floor. *Nature* 357:581–583. doi:10.1038/357581a0
- Wan F (2013) Characteristics, genesis and prospecting criteria of the Mesozoic epithermal gold deposits in Yanbian area. Masters thesis, Jilin University (in Chinese with English abstract)
- Wu TT (2013) Geological characteristics and metallogenic regularity of gold deposits from Naozhi to Duhuangling in Wangqing County, Jilin Province. Masters thesis, Jilin University (in Chinese with English abstract)
- Wu FY, Sun DY, Ge WC, Zhang YB, Grant ML, Wilde SA, Jahn BM (2011) Geochronology of the Phanerozoic granitoids in northeastern China. *J Asian Earth Sci* 41:1–30
- Yang SS, Qing M, Hao TS, Wang KY, Wan D, Piao XH, Bian HY (2010) Geological characteristics and genesis of Naozhi gold deposit, in Yanbian area, Jilin Province. *Global Geol* 29:607–613 (in Chinese with English abstract)
- Zartman RE, Doe BR (1981) Plumbotectonics—the model. *Tectonophysics* 75:135–162. doi:10.1016/0040-1951(81)90213-4
- Zeng QD, Wang ZC, He HY, Wang YB, Zhang S, Liu JM (2014) Multiple isotope composition (S, Pb, H, O, He, and Ar) and genetic implications for gold deposits in the Jiapigou gold belt, Northeast China. *Miner Deposita* 49:145–164. doi:10.1007/s00126-013-0475-2
- Zhai W, Sun XM, He XP, Su LW, Wu YL (2006) Noble gas isotopic geochemistry of Axi gold deposit, and its metallogenic implications, Xinjiang, China. *Acta Petrol Sin* 22:1–7
- Zhang YB (2002) The isotopic geochronologic frame of granitic magmatism in Yanbian area. Ph.D. thesis, Jilin University (in Chinese with English abstract)
- Zhang Y (2010) Gold deposit geological characteristics and exploration potential of the Miantian-Naozhi region. *Sci Technol West Chin* 9: 4–7 (in Chinese with English abstract)
- Zhang YB, Wu FY, Wilde S, Zhai MG, Lu XP, Sun DY (2004) Zircon U–Pb ages and tectonic implications of ‘Early Paleozoic’ granitoids at Yanbian, Jilin Province, northeast China. *Island Arc* 13:484–505. doi:10.1111/j.1440-1738.2004.00442.x
- Zhao HG (2007) Study on the metallogenesis and models in Mesozoic epithermal gold deposits in Yanbian, Jilin Province. Ph.D. thesis, Jilin University (in Chinese with English abstract)